Hindawi Publishing Corporation
International Journal of Photoenergy
Volume 2012, Article ID 804840, 11 pages
doi:10.1155/2012/804840

Research Article

Hierarchical CuO/ZnO Membranes for Environmental Applications under the Irradiation of Visible Light

Zhaoyang Liu, Hongwei Bai, and Darren Delai Sun

School of Civil & Environmental Engineering, Nanyang Technological University, Singapore 639798

Correspondence should be addressed to Zhaoyang Liu, zyliu@ntu.edu.sg and Darren Delai Sun, ddsun@ntu.edu.sg

Received 19 June 2011; Accepted 14 September 2011

Academic Editor: Jae Sung Lee

Solar visible light is a source of clean and cheap energy. Herein, a new kind of hierarchical CuO/ZnO nanomaterial was synthesized using a facile process. Characterized by FESEM, TEM, XRD, XPS, and so forth, this CuO/ZnO naomaterial shows a special hierarchical nanostructure with CuO nanoparticles grown on ZnO nanorods. By assembling the hierarchical CuO/ZnO nanomaterials on a piece of commercial glassfiber membrane, a novel hierarchical CuO/ZnO membrane was fabricated. This CuO/ZnO membrane demonstrated excellent environmental applications, such as improved photodegradation of contaminants and antibacterial activity, under the irradiation of visible light. Compared with pure ZnO nanorod membrane, the improved photodegradation and antibacterial capacities of this hierarchical CuO/ZnO membrane result from the special hierarchical nanostructure of CuO/ZnO nanomaterials, which could enhance light utilization rate, enlarge specific surface area, and retard the recombination of electrons and holes at the interfacial between CuO and ZnO. This hierarchical CuO/ZnO membrane is also easy to be regenerated by completely mineralizing the adsorbed contaminants under the irradiation of visible light. All the above characteristics of this hierarchical CuO/ZnO membrane indicate its great potential in environmental applications with solar visible light.

1. Introduction

Widespread water source contamination and increasing demand for consumable water necessitate a novel and sustainable approach to the remediation of polluted water [1]. Photocatalytic nanomaterials have shown high efficiency in contaminant removal through the degradation of organic contaminants and the inactivation of bacteria [2–4]. Solar energy is a clean and renewable resource ideal for environmental and sustainable applications. Photocatalytic degradation utilizing visible light radiation is an increasingly popular research topic [5]. ZnO is an extensively studied semiconductor employed in the photocatalytic removal of contaminants in water [6, 7]. However, pure ZnO nanomaterials have limited efficiency because of the low light utilization rates resulting from the wide-band gap (3.2 eV). ZnO nanomaterials absorb only a small portion of light in the UV spectrum and exhibit rapid recombination of electrons and holes reducing their photocatalytic activity [8, 9]. The key to broadening the applications for ZnO nanomaterials lies in overcoming these shortcomings. Over several decades, efforts have been made to enhance the photocatalytic activity of ZnO through metal [10] or carbon/nitrogen doping [4, 11]. ZnO nanomaterials have also been coupled with narrow-band gap semiconductors like Fe_2O_3, WO_3, CdS, Cu_2O, and CuO in attempts to improve photocatalytic activity by encouraging red shift [12–16]. The resulting increase in wavelength produces light in the visible spectrum, thereby, increasing light absorption and retarding electron and hole recombination. ZnO has also received attention for its antibacterial properties through a mechanism which destroys the cell membrane affecting bacterial morphology and the efflux of intracellular components [3].

Hierarchically structured nanomaterials with multiscaled organizations increase light reflection and absorption inside the material to enhance light utilization rate and enlarge specific surface area [17]. This effectively increases contaminant attachment and adsorption. These attributes make hierarchical nanomaterials a desirable approach to enhancing photocatalytic activity [18].

In practical application, the recovery of the photocatalyst from treated water is an important economic and sustainability consideration. The incorporation of the photocatalyst into a functional membrane is an ideal approach as it facilitates convenient recovery and regeneration whilst degrading foulants retained in pores or on the membrane surface by simple irradiation using either UV or visible light [19, 20]. It is meaningful to fabricate a multifunctional membrane for contaminant removal via photodegradation and inactivation of bacterial under the irradiation of visible light. The multiple functions of such a membrane comes from the functional layer created by a hierarchical structured CuO/ZnO materials, which could demonstrate high photocatalytic activity because of the enhanced light utilization rate, enlarged specific surface area, and the efficient antirecombination of electrons and holes. In this case, the photocatalysts are easy for reuse, and the multiple functional membrane is easy to be regenerated after complete mineralization of the adsorbed contaminants via extending the irradiation time of visible light.

In this study, a new kind of hierarchical CuO/ZnO nanomaterials is synthesized using low-temperature hydrothermal and photodeposition process. A piece of multifunctional membrane is fabricated by assembling the hierarchical CuO/ZnO nanomaterials on top of a piece of commercial glassfiber membrane. Under the irradiation of visible light, this functional membrane demonstrated better photodegradation of contaminants and bacterial inactivation over a comparative functional membrane with a pure ZnO layer. This membrane is also characteristically easy to regenerate and has high reusability. All the above characteristics indicate its good potential in environmental purification with the usage of solar energy.

2. Experimental Section

2.1. Materials Synthesis

2.1.1. The Synthesis of ZnO Nanorods. Zinc acetate dihydrate ($Zn(CH_3COO)_2, 2H_2O$) was purchased from Alfa, hexamethylenetetramine (HMTA: $C_6H_{12}N_4$) was purchased from Sigma, and copper sulfate ($Cu(SO_4)_2 \cdot 5H_2O$) was from Alfa. Other chemicals were purchased from Sigma. According to the reports [21–23], a mixed solution of 0.03 M $Zn(CH_3COO)_2$ and 0.03 M HMT was well prepared, and adjusted the pH of the solution around 7.5. 100 mL-mixed solution was filled in a high temperature resistance glass bottle (<140°C) and sealed tightly. After hydrothermally treated for 6 h–12 h at 95°C, the precipitation at the bottom of the glass bottle was collected and sufficiently washed for further characterization and usage.

2.1.2. The Synthesis of CuO/ZnO Hierarchical Nanomaterials. A given amount of hydrothermally synthesized ZnO nanorods were dispersed in 100 mL deionized (DI) water. 0.1 g $Cu(SO_4)_2$, $5H_2O$, and 0.1 g NaCl were added in the solution and were continuously stirred for 10 min and ultrasonicated for another 10 min to make a mixed solution [24]. A weak black UV light with a predominant wavelength of 365 nm was suspended at the middle of the solution [25]. Under the continuous stirring, the mixed solution was illuminated for 6–12 h. Collect the precipitations at the bottom and wash them with DI water sufficiently. After being calcined at 500°C for 1 h in a furnace under atmospheric condition, the samples were ready for further characterizations and environmental application tests.

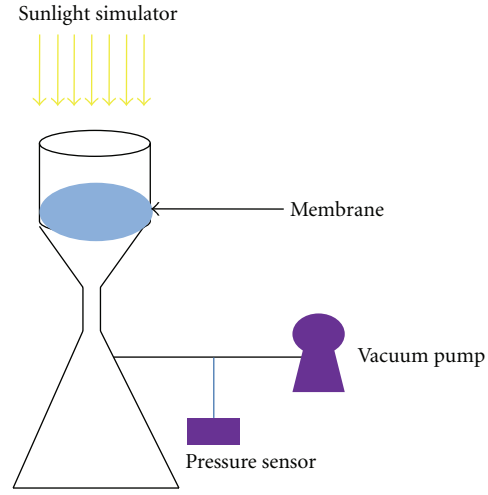

Scheme 1: Schematic setup for membrane assembly and photodegradation of contaminants.

2.1.3. Assembly of the Hierarchical CuO/ZnO Multifunctional Membrane. 100 mg of synthesized hierarchical CuO/ZnO nanomaterials were dispersed in 100 mL DI water. One piece of commercial glass fiber membrane (Adventc discs Ø 47 mm, 0.50 μm) was mounted at the bottom of the vacuum filtration cup (Scheme 1), then slowly poured the mixed solution into the filtration cup and switched on the vacuum pump. After certain time, the water was filtrated away, leaving a uniformly assembled membrane with the CuO/ZnO hierarchical materials. This membrane is named as CuO/ZnO membrane. As a comparison, a piece of pure ZnO membrane with ZnO nanorods was assembled by the same method; this membrane is named as ZnO membrane.

2.1.4. Photodegradation Test. Three kinds of commonly used pollutants, including methyl blue (MB), acid orange (AO7), and Rhodamine B (RhB) aqueous solution, were used for the test. The experiment detail was as follows. Firstly, the aqueous solutions of MB (100 mg/L), AO7 (50 mg/L), and RhB (50 mg/L) were prepared, respectively; then the solution (50 mL) was poured into the filtration cup, at the bottom of which the CuO/ZnO membrane was mounted, then let it adsorb for 1 h to reach adsorb equilibrium. Then switch on the sunlight simulator (100 mA) to start the photodegradation experiment. The whole test system is a continuous process. At a given internal, 3 mL reactant solution was drawn with a syringe, and its UV-visible adsorption value was measured by a UV-visible photospectrometer. As

a comparison, the photodegradation ability of ZnO membrane was also tested using the same methods as above.

The concurrent photocatalysis and membrane filtration experiment was conducted, and the permeate quality was monitored by measuring the UV-visible adsorption value of the collected permeate at a given internal.

The photolysis experiment without CuO/ZnO nanomaterials and ZnO nanorods was also carried out before each photodegradation experiment.

2.1.5. Antibacterial Test. Microorganism (*E. coli*) was cultivated in sterilized LB broth culture and then incubated overnight at 37°C with a shaking incubator. The concentration of *E. coli* was 10^7 CFU/mL. Before the antibacterial test, one new CuO/ZnO membrane was assembled, and then the whole vacuum filtration setup except the sunlight simulator was sterilized in a UV-sterilization fume hose. The antibacterial capability of the CuO/ZnO membrane was investigated with/without the irradiation of visible light after 40 mL *E. coli* solution was poured into the filtration cup (without switching on the vacuum pump). At an internal of 5 min, 1 mL reactant solution was drawn with a sterilized syringe and uniformly streaked on the well-solidified agar nutrient plate. After overnight's cultivation at 37°C, the colonies were counted.

At the same time, the antibacterial capability of the ZnO membrane and the blank control experiment (without CuO/ZnO nanomaterials and ZnO nanorods) with/without the irradiation of visible light were also carried out using the same methods as above.

2.1.6. Characterizations. The structure and the crystal phase of the synthesized ZnO nanorods, and the CuO/ZnO hierarchical nanomaterials were analyzed by powder X-ray diffractometer (XRD, Bruker AXS D8 advance) with monochromated high-intensity Cu Kσ radiation (λ = 1.5418 Å) operated at 40 kV and 30 mA. The obtained XRD spectra were matched with a powder diffraction file (PDF) database maintained by the International Centre for Diffraction Data (ICDD). The morphology of the samples was characterized by field emission scanning electron microscopy (FESEM, JEOL JSM-6360F) and high resolution transmission electron microscopy (HRTEM, Jeol JEM-2010). The element contents of the samples were measured by energy dispersive X-ray spectrometer (EDS) attached to the SEM. The UV-Vis diffuse reflectance spectra of the samples were measured by a Thermo Scientific Evolution 300 UV-Vis spectrophotometer (Thermo Fisher Scientific, Mass, USA) equipped with an integrating sphere assembly and a Xenon lamp source. $BaSO_4$ was used as the reflectance standard. The BET specific surface areas of the samples were determined at liquid nitrogen temperature (77 K) using a Micromeritics ASAP 2040 system. Before the measurement, 0.1 g sample was outgassed under vacuum for 6 h at 250°C.

XPS analysis was carried out at room temperature in an ultra high vacuum (UHV) chamber with a base pressure below 2.66×10^{-7} Pa. Photoemission spectra were recorded by a Kratos Axis Ultra spectrometer (Shimadzu Corporation, Kanagawa, Japan) with a monochromatic Al Kα excitation source ($h\nu$ = 1486.71 eV). Curve fitting was performed using a nonlinear least square Gaussian-Lorenzian function. Carbon calibration shift was carried out at 284.6 eV to remove the presence of residual adventitious carbon.

3. Results and Discussions

The morphology of the hydrothermally synthesized ZnO nanorods was observed by FESEM in Figure 1(a). It can be seen that the ZnO nanorod has a length of 10 to 20 μm, and the average diameter is around 1 μm, so the aspect ratio of length to diameter was around 10 to 20, which belongs to a typical rod-like structure. And the synthesized ZnO nanorod has a smooth surface with a hexagonal end. The HRTEM image in Figure 1(b) obviously confirmed that ZnO grew along the direction of [0001] plane forming a rod like structure with a typical lattice of 0.52 nm.

With the illumination of weak black light on the mixed solution of copper sulfate, sodium chloride, and ZnO nanorods, Cu nanoparticles were uniformly deposited on the surface of the ZnO nanorods. The CuO/ZnO nanomaterials were well observed by FESEM as shown in Figures 2(a)–2(c) at different magnifications. These Cu nanoparticles are supposed to nucleate from the defect parts of the ZnO nanorods and grow up. After the illumination, the ZnO nanorods were thoroughly covered by Cu nanoparticles, forming a "corn-like" architecture. The followed calcination at 500°C for 1 h makes Cu become CuO without changing the morphology of the Cu nanoparticles, as shown in Figure 2(a). The sizes of the CuO nanoparticles were around 100 nm. From Figure 2(b), it is found that only partial surface of the ZnO nanorod was covered by CuO nanoparticles. The distance between individual CuO nanoparticle was in the range of nanoscale, but the distance between individual CuO/ZnO nanorod was in the range of microscale. Therefore, these CuO/ZnO nanomaterials form a kind of hierarchical structure, which possesses the advantages of promoting mass transfer, enlarging the specific surface area, and promoting the charge transfer from ZnO nanorod to CuO nanoparticle. The energy disperse X-ray spectrum of the CuO/ZnO hierarchical material (Cu (10 wt%)) in Figure 2(c) clearly proved that the elements of Zn, O, and Cu dominate the composition of these novel hierarchical materials. Further quantitative analysis of the EDS reveals that the atomic ratio of O : Zn : Cu is about 10 : 9 : 1, indicating that the stoichiometric [(Zn + Cu)/O = 1 : 1] CuO/ZnO hierarchical nanomaterial is consisted of ZnO and CuO.

The X-ray diffractometer was employed to measure the crystallization of the hydrothermally synthesized ZnO nanorods and the CuO/ZnO hierarchical nanomaterials. As shown in Figure 3, the hydrothermally synthesized ZnO nanorods were crystallized into a standard hexagonal structure (JCPDS 89–1397) [26]. After CuO was formed on the ZnO nanorod, all the dominant peaks of the original ZnO nanorods were kept, but the peaks of CuO (002) and CuO (110) at $2\theta = 39.2^\circ$ and $2\theta = 32.6^\circ$ appears respectively, and the overlapped peaks of CuO (111) and ZnO (101) around $2\theta = 36.4^\circ$ also revealed the existence of CuO in this material and further confirmed that the CuO nanoparticles

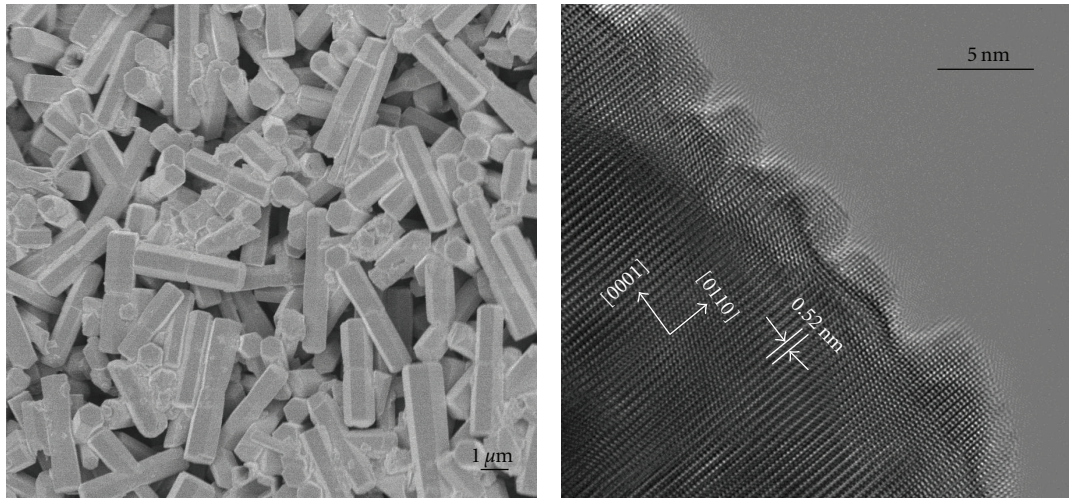

(a) (b)

Figure 1: (a) FESEM image and (b) HRTEM image of the hydrothermally synthesized ZnO nanorods.

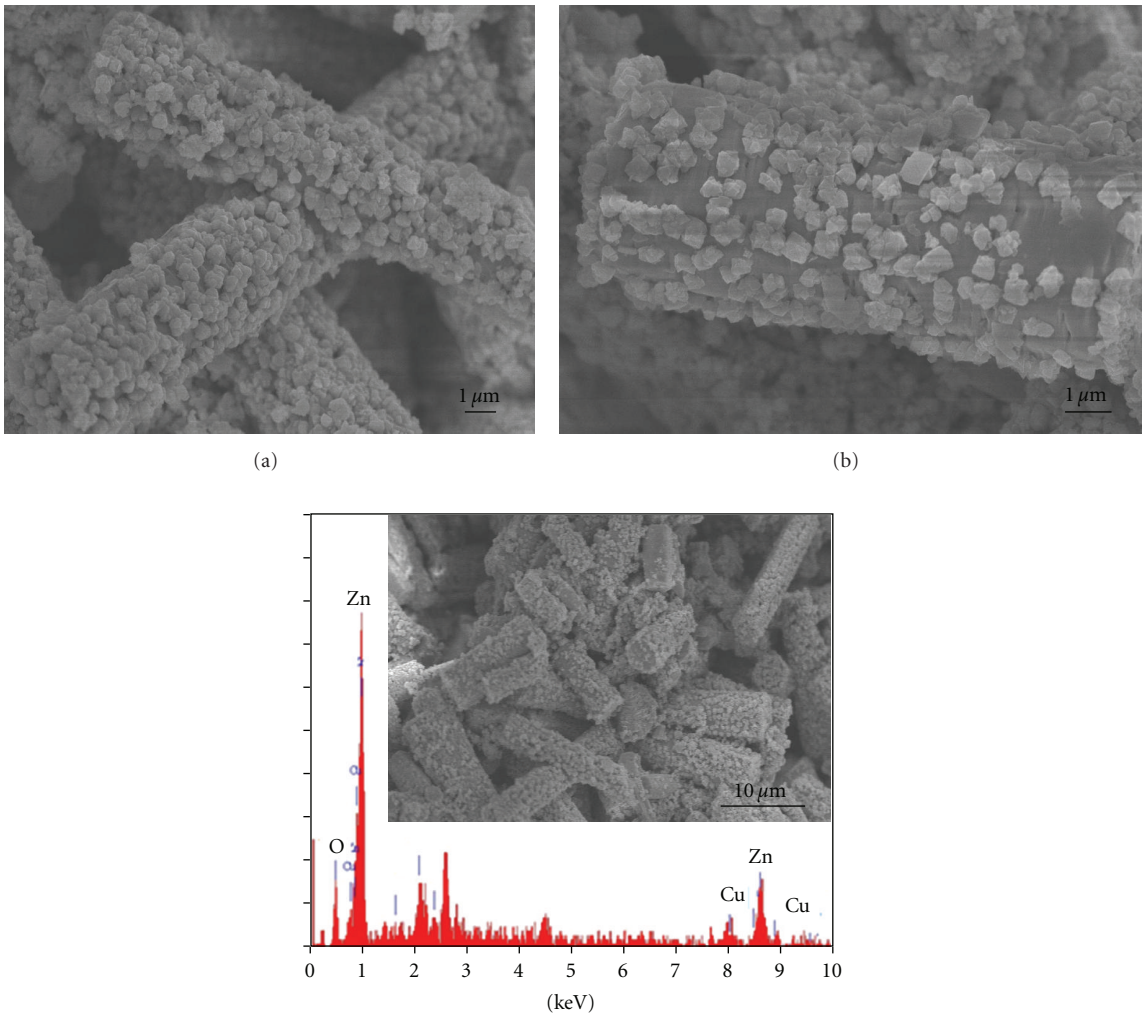

(a) (b)

(c)

Figure 2: (a)-(b), FESEM images of the hierarchical CuO/ZnO nanomaterials at different magnifications, (c) the EDS spectrum of the hierarchical CuO/ZnO nanomaterials, insert is an overview SEM image.

Table 1: Binding energies (eV), fwhm of the hierarchical CuO/ZnO nanomaterials.

	Position (fwhm)		Position (fwhm)		Position (fwhm)	
	O 1s	O 1s	Zn $2p_{3/2}$	Zn $2p_{1/2}$	Cu $2p_{3/2}$	Cu $2p_{1/2}$
CuO/ZnO hierarchical nanomaterials	530.508 (2.009)	532.265 (2.643)	1021.45 (3.162)	1044.44 (3.027)	934.832 (3.559)	954.913 (3.656)

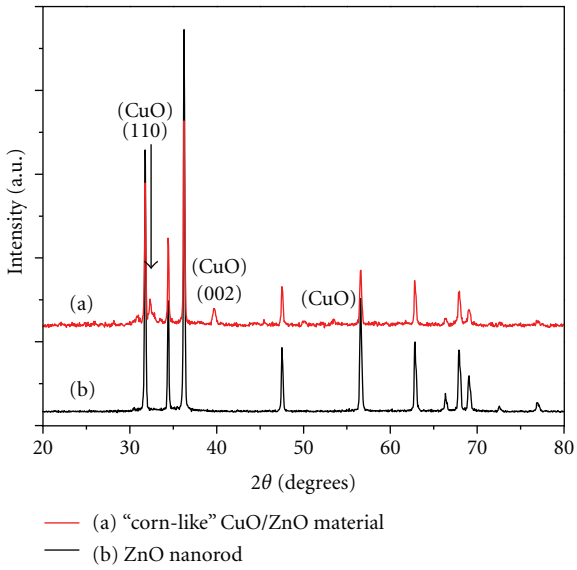

Figure 3: XRD patterns of the pure ZnO nanorods and the hierarchical CuO/ZnO nanomaterials.

were uniformly distributed on the surface of this material [27–29].

The chemical composition and electronic structure of the CuO/ZnO hierarchical nanomaterials was investigated by X-ray photoelectron spectroscopy (XPS). The XPS spectra of the Cu 2p, Zn 2p, and O 1s were presented in Figure 4 while the detailed binding energies (eV) and their corresponding full width at half maximum (fwhm) were listed in Table 1. The characteristic intense peaks were centered at 1021.45 eV (Zn 2p3/2) and 1044.44 eV (Zn 2p1/2) from XPS spectra of Zn 2p in Figure 4(a), clearly indicating that the oxidation state of Zn is +2 in the form of ZnO on the surface of the CuO/ZnO hierarchical nanomaterials [30]. The characteristic peaks were located at 934.832 (Cu 2p3/2) and 954.913 (Cu 2p1/2), and their corresponding satellite peaks of the Cu 2p XPS spectra presented in Figure 4(b), obviously confirming that the oxidation state of Cu is +2 in the form of CuO on the surface of the CuO/ZnO hierarchical nanomaterials [31–33]. The broad O 1s peak in Figure 4(c) was comprised of two small peaks, one is located at 530.508 eV and the other one is located at 532.265 eV. The former is inherent O atoms bound to metals such as Cu and Zn, while the latter peak resulted from the possible surface contaminations by hydroxyl species and carbonate species [34].

The UV-visible spectra of the CuO/ZnO hierarchical nanomaterials and ZnO nanorods were presented in Figure 5. Obviously, the CuO/ZnO hierarchical nanomaterials displayed a stronger UV absorption ability over ZnO nanorods in both UV and visible ranges, which indicates that the UV-visible absorption spectra has been red shifted to visible range. This is because (1) on one hand, the rough surface of the CuO/ZnO hierarchical nanomaterials would allow more light reflection and absorption inside the structure [18], which is different from the smooth surface of ZnO nanorods; (2) on the other hand, CuO has a potential to red-shift the light absorption spectrum to visible range [16].

The N_2 adsorption/desorption isotherm curve of the CuO/ZnO hierarchical nanomaterials was measured as shown in Figure 6. Clearly, the CuO/ZnO hierarchical nanomaterials show the characteristic mesoporous materials, [35] which is favorable for the mass transfer, light reflection, and bacterial attachment [36]. As measured, the specific surface area of the CuO/ZnO hierarchical nanomaterials is 11.24 m^2/g, which is much higher than that of ZnO nanorods (4.81 m^2/g) and that of commercial ZnO powder (3 m^2/g) [35].

3.1. Photodegradation of Contaminants by the Multifunctional CuO/ZnO Membrane. The CuO/ZnO membrane, assembled by depositing CuO/ZnO nanomaterials on a glassfiber membrane, was tested for the removal of contaminants by photodegradation and filtration. As a blank control, commercial ZnO powder and physically mixed CuO/ZnO nanoparticles were also depositing on glassfiber membranes to investigate their photodegradation abilities of contaminants. Firstly, the photodegradation of industrial dye, such as MB, under the irradiation of visible light on the surface of CuO/ZnO membrane was investigated, as shown in Figure 7. MB solution with an initial concentration of 100 ppm was completely degraded after visible light irradiation for 60 min (Figure 7(a)). The CuO/ZnO membrane demonstrated better photodegradation ability compared with ZnO membrane and physically mixed CuO/ZnO membrane under the same conditions (Figure 7(b)) because of the special hierarchical CuO/ZnO "corn-like" nanostructure [37]. After switching on the vacuum pump as shown in Scheme 1, the MB solution was removed by the concurrent photodegradation and filtration through the assembled membranes. By measuring the permeate from CuO/ZnO membrane, MB was found to be totally removed (after 60 min reaction), but there was still about 60% MB remaining in the permeate from ZnO membrane (Figure 7(b)). Moreover, the CuO/ZnO membrane is easy to be regenerated after the adsorbed MB was completely degraded by extending the visible light irradiation time.

The CuO/ZnO membrane and ZnO membrane were also tested for the removal of AO7 (Figure 8). The AO7 solution (initial concentration of 50 mg/L and pH of 7) was completely photodegraded by the CuO/ZnO membrane after 90 min irradiation of visible light, but longer

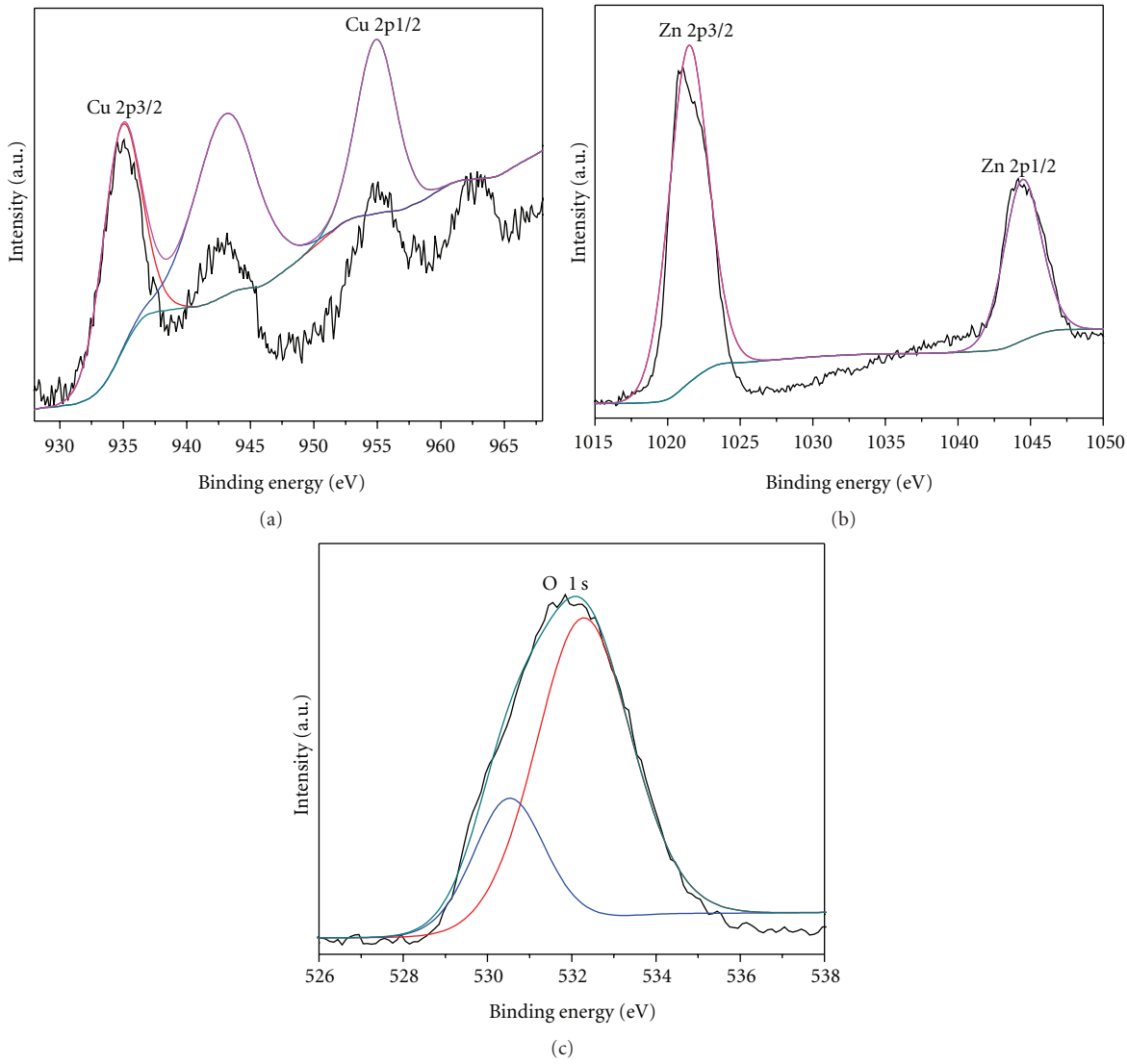

Figure 4: XPS spectra of the Cu 2p, Zn 2p, and O 1s state on the surface of the hierarchical CuO/ZnO nanomaterials.

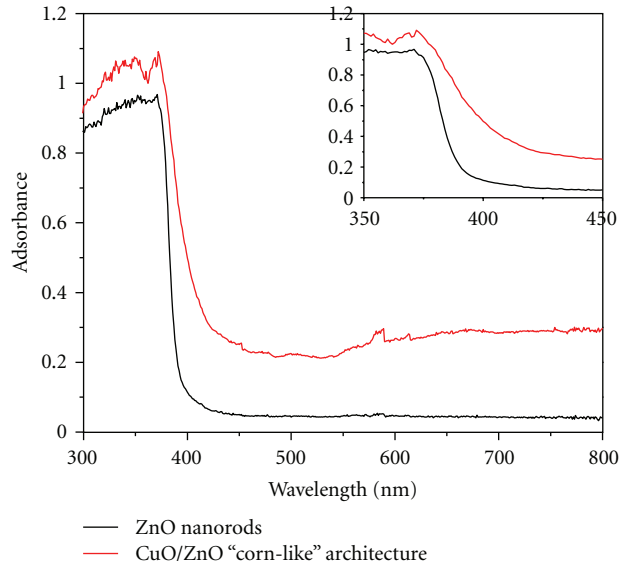

Figure 5: The UV-visible spectra of the hierarchical CuO/ZnO nanomaterials and ZnO nanorods.

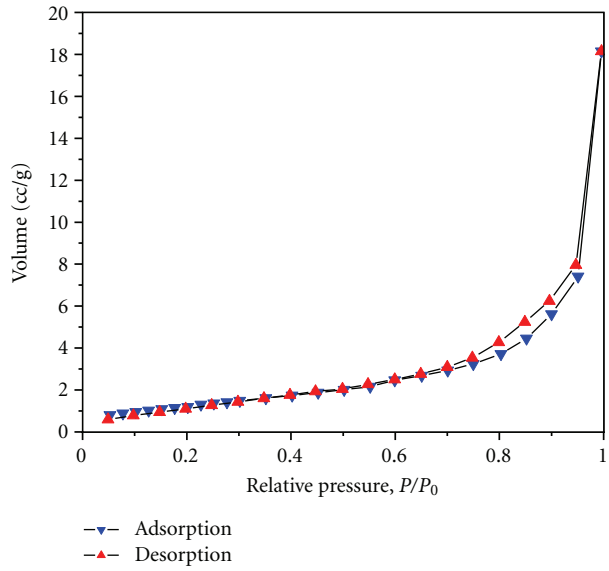

Figure 6: N_2 adsorption/desorption isotherm curve of the hierarchical CuO/ZnO nanomaterials.

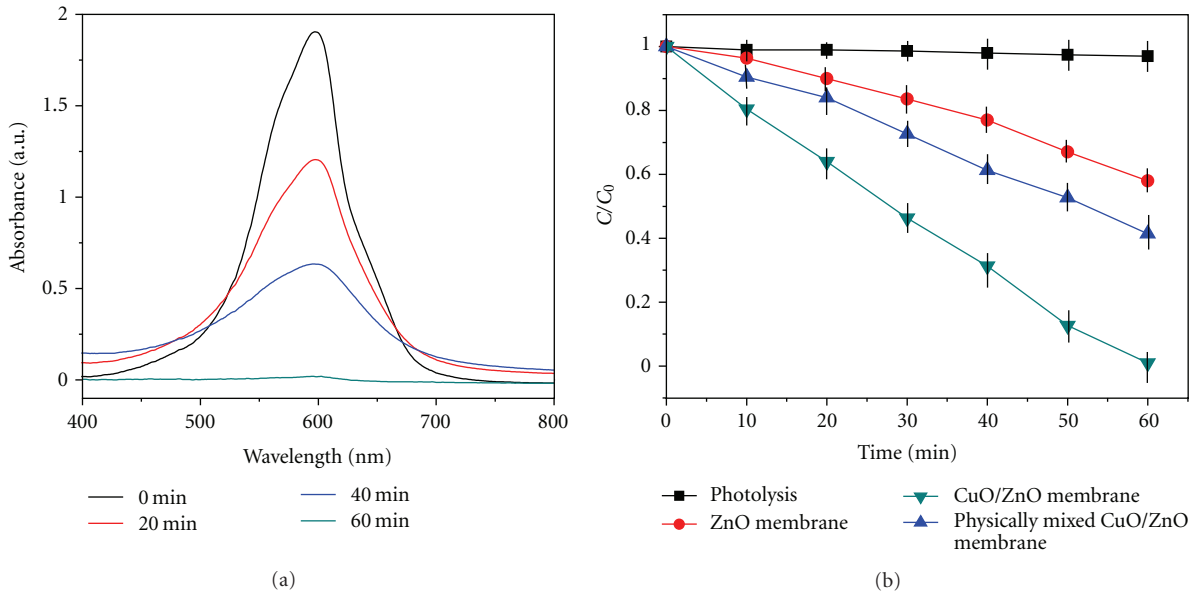

Figure 7: (a) The absorption spectra of MB solution under the irradiation of visible light on the CuO/ZnO membrane, and (b) the concentration change of MB solution under the irradiation of visible light on the CuO/ZnO membrane and ZnO membrane.

time is needed for the complete degradation of AO7 by the ZnO membrane. Through measuring the concentration change of AO7 during the visible light irradiation process, the CuO/ZnO membrane demonstrated better photodegradation ability than that of ZnO membrane under the same condition (Figure 8(b)). The concurrent membrane filtration and photocatalysis of AO7 was also investigated, no AO7 was found in the permeate from CuO/ZnO membrane (after 90 min), while there was still 63% AO7 found in the permeate from the ZnO membrane because of pure ZnO's low photodegradation ability. At the same time, the CuO/ZnO membrane is easy for regeneration after complete photodegradation of AO7 adsorbed on the surface of CuO/ZnO membrane by extending the irradiation time of visible light.

The CuO/ZnO membrane and ZnO membrane was also tested for the removal of dye contaminant RhB, the concentration of RhB was monitored by measuring the UV-visible adsorption value at 553 nm. The concentration change of RhB under the irradiation of visible light on the CuO/ZnO membrane and ZnO membrane was presented in Figure 9. Obviously, the CuO/ZnO membrane demonstrated better photodegradation ability compared with ZnO membrane. After 120 min irradiation of visible light, the CuO/ZnO membrane completely degraded the RhB in the solution, while ZnO membrane only degraded about 45%.

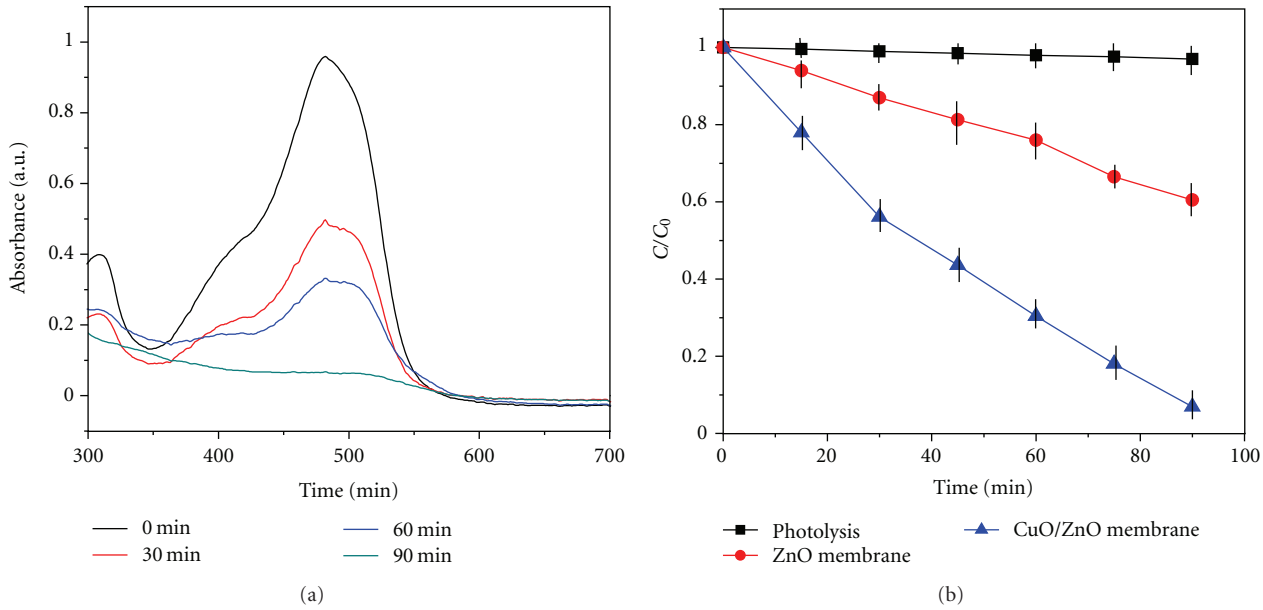

Figure 8: (a) The absorption spectra of AO7 solution under the irradiation of visible light on the CuO/ZnO membrane, and (b) the concentration change of AO7 solution under the irradiation of visible light on the CuO/ZnO membrane and ZnO membrane.

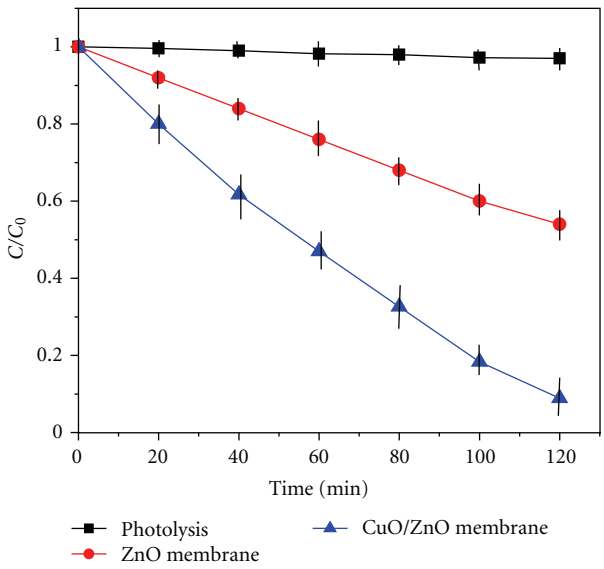

Figure 9: The concentration change of RhB under the irradiation of visible light on the CuO/ZnO membrane and ZnO membrane.

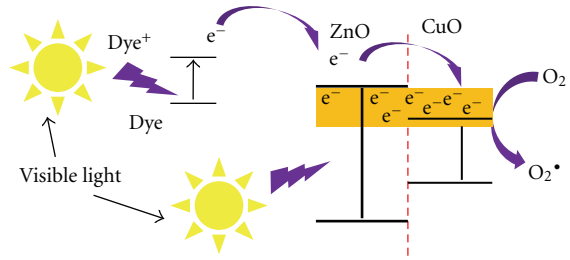

Scheme 2: Schematic diagram of the electron transfer and the energy band positions of ZnO and CuO in the hierarchical CuO/ZnO materials for the photodegradation of dye contaminants under the irradiation of visible light.

The enhanced photodegradation ability of CuO/ZnO membrane was attributed to the following reasons. Firstly, the enlarged specific surface area of CuO/ZnO nanomaterials (11.24 m^2/g) over that of ZnO nanorods (4.81 m^2/g) is favorable for contaminant adsorption, providing more reaction sites for the photocatalytic reactions. Secondly, the CuO/ZnO nanomaterials improved the light utilization rate compared with ZnO nanorods. The rough surface of CuO/ZnO nanomaterials can enhance the light reflection and absorption inside the CuO/ZnO nanomaterials, while on the contrast, ZnO nanorods only can be excited by UV light which just accounts for a minor part of the solar light [16]. Moreover, the CuO/ZnO hierarchical nanomaterial with larger specific surface area favors the adsorption of dye contaminants, the adsorbed dye contaminants is favorable for the utilization of visible light [38, 39], and the produced electrons and holes would be transferred to CuO/ZnO nanomaterials [40]. The transferred electrons were captured by the surface adsorbed O_2 to yield $O_2^{\bullet -}$ and $HOO^{\bullet}$ radicals [40]. Then the dye contaminants are photodegraded in situ by the produced radicals. At the same time, the band gap difference between CuO and ZnO facilitates the transfer of photogenerated electrons and holes from ZnO to CuO (Scheme 2) [8]; in this way, the recombination of electrons and holes is retarded to a certain extent [41]. Therefore, the photocatalytic activity is enhanced.

3.2. Antibacterial Capability Test. Besides the photodegradation of contaminants, the antibacterial capabilities of the CuO/ZnO membrane and ZnO membrane were also investigated. Figure 10 shows the inactivation of *E. coli* on

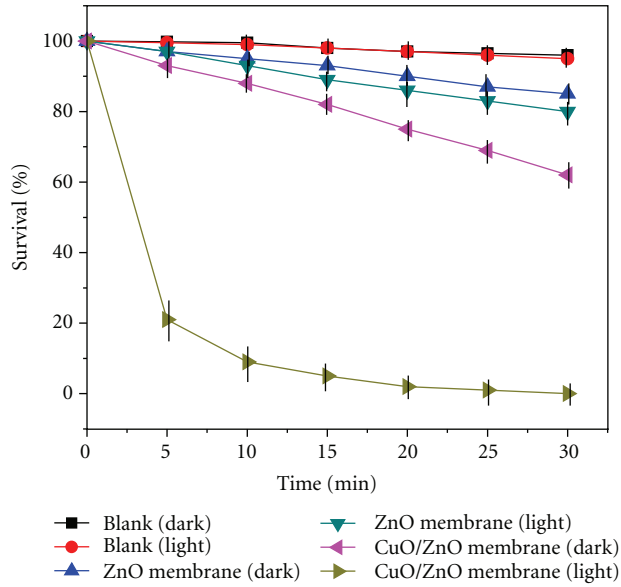

Figure 10: Plot of % *E. coli* survival rate as the function of visible light irradiation time on CuO/ZnO membrane and ZnO membrane.

the CuO/ZnO membrane and ZnO membrane with/without the irradiation of visible light. The survival of *E. coli* can be calculated by % survival $= B/A * 100$ (where A is the number of surviving microbial colonies in the control, and B is the number of surviving microbial colonies in the tested sample). To rule out the synergic effect of CuO/ZnO membrane on the inactivation of *E. coli*, both blank control experiments for the pure glassfiber membrane and inactivation of *E. coli* by ZnO membrane with/without the irradiation were conducted using the same method. It is found that the direct visible light irradiation has no obvious effect on the inactivation of *E. coli* on pure glassfiber membrane. As we know, ZnO [3] and CuO [17] have certain antibacterial growth ability; hence, both CuO/ZnO membrane and ZnO membrane demonstrated antibacterial growth in the dark as expected. However, under the irradiation of visible light, the antibacterial capability of CuO/ZnO membrane was greatly enhanced and was significantly higher than that of ZnO membrane; wherein, CuO/ZnO membrane can completely kill all the *E. coli* in the solution after 20 min irradiation of visible light, while ZnO membrane can only kill around 40% *E. coli* even after 30 min irradiation of visible light. This indicates that the synergic effect of CuO/ZnO nanomaterials played a significant role in the improvement of antibacterial capability, which is in consistent with previous reports [42]. The enhanced antibacterial capability is attributed to (1) the enlarged specific surface area and mesoporous property [36] of CuO/ZnO nanomaterial which is convenient for bacterial attachment and (2) the enhanced photocatalytic activity by enlarging the light utilization rate and retarding the recombination of photogenerated electrons and holes between CuO and ZnO, as explained in previous section [8, 16].

4. Conclusion

The hierarchical CuO/ZnO nanomaterials have been successfully synthesized for the first time by the combination of low-hydrothermal and photodeposition methods. This hierarchical CuO/ZnO nanomaterial was well characterized by FESEM, TEM, XRD, XPS, and so forth. The CuO/ZnO membrane was assembled by depositing the hierarchical CuO/ZnO nanomaterials on the surface of glassfiber membrane with the help of vacuum filtration. The CuO/ZnO membrane demonstrated high photodegradation ability for dye contaminants, such as MB, AO7, and RhB, under visible light irradiation, which results from the enlarged specific surface area for contaminants adsorption, the improved light utilization rate, and the retarded recombination of electrons and holes. At the same time, the CuO/ZnO membrane is easy for regeneration by complete degradation the adsorbed dyes with extending the visible light irradiation time. Furthermore, the CuO/ZnO membrane also demonstrated better antibacterial capability than ZnO membrane due to the synergic effect of CuO/ZnO nanomaterials. All these advantages of the CuO/ZnO membrane would bring great benefits to water purification applications.

Acknowledgment

The authors are grateful for the financial support received from the National Research Foundation/NTU Joint R&D (REF. COY-25-24/N370-4).

References

[1] M. A. Shannon, P. W. Bohn, M. Elimelech, J. G. Georgiadis, B. J. Marinas, and A. M. Mayes, "Science and technology for water purification in the coming decades," *Nature*, vol. 452, no. 7185, pp. 301–310, 2008.

[2] X. Huang, M. Leal, and Q. Li, "Degradation of natural organic matter by TiO_2 photocatalytic oxidation and its effect on fouling of low-pressure membranes," *Water Research*, vol. 42, no. 4-5, pp. 1142–1150, 2008.

[3] Q. Li, S. Mahendra, D. Y. Lyon et al., "Antimicrobial nanomaterials for water disinfection and microbial control: potential applications and implications," *Water Research*, vol. 42, no. 18, pp. 4591–4602, 2008.

[4] R. Asahi, T. Morikawa, T. Ohwaki, K. Aoki, and Y. Taga, "Visible-light photocatalysis in nitrogen-doped titanium oxides," *Science*, vol. 293, no. 5528, pp. 269–271, 2001.

[5] A. Fujishima, X. Zhang, and D. A. Tryk, "TiO_2 photocatalysis and related surface phenomena," *Surface Science Reports*, vol. 63, no. 12, pp. 515–582, 2008.

[6] X. Zhang, J. H. Pan, A. J. Du, W. Fu, D. D. Sun, and J. O. Leckie, "Combination of one-dimensional TiO_2 nanowire photocatalytic oxidation with microfiltration for water treatment," *Water Research*, vol. 43, no. 5, pp. 1179–1186, 2009.

[7] J. Yu and X. Yu, "Hydrothermal synthesis and photocatalytic activity of zinc oxide hollow spheres," *Environmental Science & Technology*, vol. 42, no. 13, pp. 4902–4907, 2008.

[8] S. Wei, Y. Chen, Y. Ma, and Z. Shao, "Fabrication of CuO/ZnO composite films with cathodic co-electrodeposition and their photocatalytic performance," *Journal of Molecular Catalysis A*, vol. 331, no. 1-2, pp. 112–116, 2010.

[9] Z. Liu, D. D. Sun, P. Guo, and J. O. Leckie, "An efficient bicomponent TiO_2/SnO_2 nanofiber photocatalyst fabricated by electrospinning with a side-by-side dual spinneret method," *Nano Letters*, vol. 7, no. 4, pp. 1081–1085, 2007.

[10] X. Qiu, G. Li, X. Sun, L. Li, and X. Fu, "Doping effects of Co^{2+} ions on ZnO nanorods and their photocatalytic properties," *Nanotechnology*, vol. 19, no. 21, Article ID 215703, 2008.

[11] S. Liu, C. Li, J. Yu, and Q. Xiang, "Improved visible-light photocatalytic activity of porous carbon self-doped ZnO nanosheet-assembled flowers," *CrystEngComm*, vol. 13, pp. 2533–2541, 2011.

[12] P. Sharma, P. Kumar, D. Deva, R. Shrivastav, S. Dass, and V. R. Satsangi, "Nanostructured Zn-Fe2O3 thin film modified by Fe-TiO2 for photoelectrochemical generation of hydrogen," *International Journal of Hydrogen Energy*, vol. 35, no. 20, pp. 10883–10889, 2010.

[13] T. Arai, M. Yanagida, Y. Konishi, Y. Iwasaki, H. Sugihara, and K. Sayama, "Promotion effect of CuO co-catalyst on WO_3-catalyzed photodegradation of organic substances," *Catalysis Communications*, vol. 9, no. 6, pp. 1254–1258, 2008.

[14] C. Lévy-Clément, R. Tena-Zaera, M. A. Ryan, A. Katty, and G. Hodes, "CdSe-sensitized p-CuSCN/nanowire n-ZnO heterojunctions," *Advanced Materials*, vol. 17, no. 12, pp. 1512–1515, 2005.

[15] N. Helaïli, Y. Bessekhouad, A. Bouguelia, and M. Trari, "p-Cu_2O/n-ZnO heterojunction applied to visible light Orange II degradation," *Solar Energy*, vol. 84, no. 7, pp. 1187–1192, 2010.

[16] B. Li and Y. Wang, "Facile synthesis and photocatalytic activity of ZnO-CuO nanocomposite," *Superlattices and Microstructures*, vol. 47, no. 5, pp. 615–623, 2010.

[17] M. Heinlaan, A. Ivask, I. Blinova, H. C. Dubourguier, and A. Kahru, "Toxicity of nanosized and bulk ZnO, CuO and TiO_2 to bacteria Vibrio fischeri and crustaceans Daphnia magna and Thamnocephalus platyurus," *Chemosphere*, vol. 71, no. 7, pp. 1308–1316, 2008.

[18] H. Bai, Z. Liu, and D. D. Sun, "Hierarchically multifunctional TiO_2 nano-thorn membrane for water purification," *Chemical Communications*, vol. 46, no. 35, pp. 6542–6544, 2010.

[19] H. Bai, X. Zhang, J. Pan, D. D. Sun, and J. Shao, "Combination of nano TiO_2 photocatalytic oxidation with microfiltration (MF) for natural organic matter removal," *Water Science and Technology*, vol. 9, no. 1, pp. 31–37, 2009.

[20] X. Zhang, A. J. Du, P. Lee, D. D. Sun, and J. O. Leckie, "TiO_2 nanowire membrane for concurrent filtration and photocatalytic oxidation of humic acid in water," *Journal of Membrane Science*, vol. 313, no. 1-2, pp. 44–51, 2008.

[21] Q. Li, V. Kumar, Y. Li, H. Zhang, T. J. Marks, and R. P. H. Chang, "Fabrication of ZnO nanorods and nanotubes in aqueous solutions," *Chemistry of Materials*, vol. 17, no. 5, pp. 1001–1006, 2005.

[22] B. Liu and H. C. Zeng, "Hydrothermal synthesis of ZnO nanorods in the diameter regime of 50 nm," *Journal of the American Chemical Society*, vol. 125, no. 15, pp. 4430–4431, 2003.

[23] X. Feng, L. Feng, M. Jin, J. Zhai, L. Jiang, and D. Zhu, 'Reversible super-hydrophobicity to super-hydrophilicity transition of aligned ZnO nanorod films," *Journal of the American Chemical Society*, vol. 126, no. 1, pp. 62–63, 2004.

[24] A. Filankembo, S. Giorgio, I. Lisiecki, and M. P. Pileni, "Is the anion the major parameter in the shape control of nanocrystals?" *Journal of Physical Chemistry B*, vol. 107, no. 9, pp. 7492–7500, 2003.

[25] K. Sunada, T. Watanabe, and K. Hashimoto, "Bactericidal activity of copper-deposited TiO_2 thin film under weak UV light illumination," *Environmental Science and Technology*, vol. 37, no. 20, pp. 4785–4789, 2003.

[26] U. Pal and P. Santiago, "Controlling the morphology of ZnO nanostructures in a low-temperature hydrothermal process," *Journal of Physical Chemistry B*, vol. 109, no. 32, pp. 15317–15321, 2005.

[27] N. Wu, M. Zhao, J. G. Zheng et al., "Porous CuO-ZnO nanocomposite for sensing electrode of high-temperature CO solid-state electrochemical sensor," *Nanotechnology*, vol. 16, no. 12, pp. 2878–2881, 2005.

[28] S. M. Zhou, X. H. Zhang, X. M. Meng et al., "The fabrication and optical properties of highly crystalline ultra-long Cu-doped ZnO nanowires," *Nanotechnology*, vol. 15, no. 9, pp. 1152–1155, 2004.

[29] G. K. Mor, O. K. Varghese, R. H. T. Wilke et al., "p-type Cu-Ti-O nanotube arrays and their use in self-biased heterojunction photoelectrochemical diodes for hydrogen generation," *Nano Letters*, vol. 8, no. 7, pp. 1906–1911, 2008.

[30] Y. Myung, D. M. Jang, T. K. Sung et al., "Composition-tuned ZnO—CdSSe Core—Shell nanowire arrays," *ACS Nano*, vol. 4, no. 7, pp. 3789–3800, 2010.

[31] Y. G. Zhang, L. L. Ma, J. L. Li, and Y. Yu, "In situ Fenton reagent generated from TiO_2/Cu_2O composite film: a new way to utilize TiO_2 under visible light irradiation," *Environmental Science and Technology*, vol. 41, no. 17, pp. 6264–6269, 2007.

[32] J. Yu and J. Ran, "Facile preparation and enhanced photocatalytic H_2-production activity of $Cu(OH)_2$ cluster modified TiO_2," *Energy and Environmental Science*, vol. 4, pp. 1364–1371, 2011.

[33] J. Yu, Y. Hai, and M. Jaroniec, "Photocatalytic hydrogen production over CuO-modified titania," *Journal of Colloid and Interface Science*, vol. 357, no. 1, pp. 223–228, 2011.

[34] J. Ng, S. Xu, X. Zhang, H. Y. Yang, and D. D. Sun, "Hybridized nanowires and cubes: a novel architecture of a heterojunctioned $TiO_2/SrTiO_3$ thin film for efficient water splitting," *Advanced Functional Materials*, vol. 20, no. 24, pp. 4287–4294, 2010.

[35] C. M. Janet, S. Navaladian, B. Viswanathan, T. K. Varadarajan, and R. P. Viswanath, "Heterogeneous wet chemical synthesis of superlattice-type hierarchical ZnO architectures for concurrent H_2 production and N_2 reduction," *Journal of Physical Chemistry C*, vol. 114, no. 6, pp. 2622–2632, 2010.

[36] H. Oveisi, S. Rahighi, X. Jiang et al., "Unusual antibacterial property of mesoporous titania films: drastic improvement by controlling surface area and crystallinity," *Chemistry*, vol. 5, no. 9, pp. 1978–1983, 2010.

[37] H. Bai, Z. Liu, and D. D. Sun, "Hierarchical ZnO/Cu "corn-like" materials with high photodegradation and antibacterial capability under visible light," *Physical Chemistry Chemical Physics*, vol. 13, no. 13, pp. 6205–6210, 2011.

[38] D. Chatterjee and S. Dasgupta, "Visible light induced photocatalytic degradation of organic pollutants," *Journal of Photochemistry and Photobiology C*, vol. 6, no. 2-3, pp. 186–205, 2005.

[39] G. Liu, G. Li, X. Qiu, and L. Li, "Synthesis of ZnO/titanate nanocomposites with highly photocatalytic activity under visible light irradiation," *Journal of Alloys and Compounds*, vol. 481, no. 1-2, pp. 492–497, 2009.

[40] K. Vinodgopal, D. E. Wynkoop, and P. V. Kamat, "Environmental photochemistry on semiconductor surfaces: photosensitized degradation of a textile azo dye, Acid Orange 7, on TiO_2 particles using visible light," *Environmental Science and Technology*, vol. 30, no. 5, pp. 1660–1666, 1996.

[41] G. Li, N. M. Dimitrijevic, L. Chen, T. Rajh, and K. A. Gray, "Role of surface/interfacial Cu^{2+} sites in the photocatalytic activity of coupled CuO-TiO_2 nanocomposites," *Journal of Physical Chemistry C*, vol. 112, no. 48, pp. 19040–19044, 2008.

[42] H. Kong, J. Song, and J. Jang, "Photocatalytic antibacterial capabilities of TiO_2-biocidal polymer nanocomposites synthesized by a surface-initiated photopolymerization," *Environmental Science & Technology*, vol. 44, no. 14, pp. 5672–5676, 2010.